Passive Impedance Control of Robots with Viscoelastic Joints via Inner-loop Torque Control

Min Jun Kim[1,2], Alexander Werner[2,3], Florian Loeffl[2] and Christian Ott[2]

***Abstract*—This paper presents passive impedance control of flexible joint robots (FJRs) via inner-loop torque control of elastic joints. However, according to our theoretical analysis, the torque control methods of series elastic actuators (SEAs) are often limited by the fact that the acceleration signals are amplified by the control gains. Since the acceleration signals are often affected by differentiation noise, the analysis may become invalid in practice. To alleviate this limitation, we propose the use of the so-called series viscoelastic actuator (SvEA), which significantly reduces the acceleration amplification. Consequently, in contrast to the SEA case, the theoretical analysis of an SvEA-based FJR is valid in real implementations. We would like to highlight the fact that the theoretical analysis (more specifically, passivity analysis) is performed for nonlinear robot dynamics without linearization. As a result, the passive impedance controller can be realized more robustly with enhanced inner-loop torque control.**

***Index Terms*—Joint torque control, impedance control, series elastic actuator, SEA, series viscoelastic actuator, SvEA**

I. Introduction

INTENTIONAL elasticity in robot joints is one of the major trends in robotics. While compliant behaviors can be realized through torque sensing and control, intrinsic compliance enables even more robust behavior. In this regard, flexible joint robots (FJRs) equipped with series elastic actuators (SEAs) are becoming increasingly common because they combine torque sensing and mechanical robustness [1]–[7]. Joint torque control of SEA is one of the most important research areas because, conceptually, it allows generation of arbitrary link-side behavior.

In particular, in this paper, an impedance controller is realized on the link-side of FJRs using a cascaded inner-loop joint torque controller (Fig. 1). However, stability of the inner-loop does not necessarily imply stability/passivity of the entire system. The effect of link-side dynamics can be neglected in the analysis only if the torque dynamics are fast enough; note that this is why electric motors can be considered as torque sources. Physically speaking, the torque dynamics of the electric motors are very fast because the value of the inductance (which is analogous to mechanical mass) is negligibly small. However, unlike electric motors, the SEA often has large reflected inertia, so its own dynamics are hard to neglect. Namely, even if the inner torque control loop is stable (τ_d to τ_j in Fig. 1), the link-side impedance control may not be stable/passive.

This work was supported by the National Research Foundation of Korea (NRF) grant funded by the Korea government(MSIT) (No. 2021R1C1C1005232), and by the European Research Council (ERC) under the European Union's Horizon 2020 research and innovation programme (grant agreement No. 819358).

[1] Department of Electrical Engineering, KAIST, South Korea.

[2] Institute for Robotics and Mechatronics, German Aerospace Center (DLR), Germany.

[3] Department of Electrical and Computer Engineering, University of Waterloo, Canada.

E-mail address: minjun.kim@kaist.ac.kr.

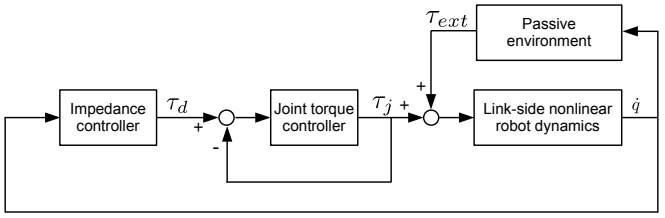

Fig. 1. Overview of the control scheme. Link-side impedance behavior is realized by cascade of impedance controller and joint torque controller.

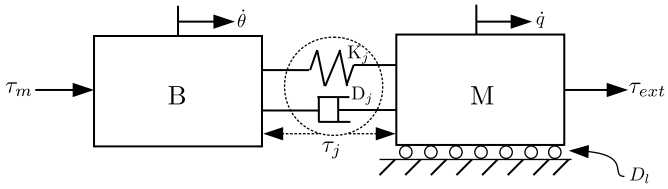

Fig. 2. Schematic diagram of a SvEA. It becomes SEA when $D_j = 0$.

This paper claims that SEA torque control approaches have practical limitation of excessive acceleration feedback. To alleviate this, additional viscous element can be introduced parallel to the elastic element, as shown in Fig. 2. This particular mechanism is hereinafter called series viscoelastic actuator (SvEA). With SvEA, passive impedance controller can be realized on the link-side more robustly.

Before presenting the main contributions, we present a thorough literature review for main keywords of this paper in the following.

A. Impedance control of FJR via torque control

A schematic diagram of an SEA- or SvEA-based FJR is shown in Fig. 2. To realize impedance behavior on the FJR, there are two major approaches; the first approach employs motor-side variable (θ) feedback, and the other one employs link-side variable (q) feedback. Impedance control with θ-feedback [8]–[11] is known to have clear physical interpretation that leads to passivity properties by virtue of collocation. However, a θ-feedback impedance controller renders spring-damper behavior to the motor-side rather than the link-side. [12] proposed a damping design considering the link-side motion but only under a quasistatic assumption.

To directly access the link-side dynamics, the most straightforward method is to feedback linearize the system to obtain the 4th order differential equation with respect to q [13], [14]. By doing so, we can arbitrarily shape the behavior of the link-side variable q. These approaches, however, require high order derivatives of q (greater than three), which might be burdensome for real implementation.

One way to avoid this difficulty is to employ cascade control schemes that make the joint torque τ_j follow a user-defined desired joint torque τ_d. With an inner-loop torque controller, in principle, any rigid-body controller can be employed as an outer-loop controller. This paper is particularly interested in an impedance controller consisting of PD action and gravity compensation.

To summarize, as shown in Fig. 1, this paper aims at realizing an outer-loop link-side impedance controller by utilizing an inner-loop torque controller. In the next subsection, various inner-loop SEA torque control methods are reviewed.

B. Torque control methods of SEAs

If the inner-loop torque tracking dynamics are dominantly fast, then we can assume $\tau_j \equiv \tau_d$ in Fig. 1, meaning that the desired link-side behavior is perfectly achieved. However, as addressed earlier, the inner-loop dynamics are not sufficiently fast to dominate the other sub-dynamics, and therefore, the stability and passivity of the entire system are not easily guaranteed. Stability is a fundamental property of a controlled system, while passivity is an additional property that plays an important role in interaction problems.[1] Moreover, In [15], it is reported that the existence of link/environmental dynamics may reduce the bandwidth of the inner-loop torque controller. Therefore, SEA torque control has been studied extensively for over a decade using various techniques, e.g., [16]–[19].

In this paper, the control methods are classified into two categories: torque control via direct feedback (TC-DF) and torque control via velocity source (TC-VS). In TC-DF, torque tracking error is used directly in the control law, e.g., PID of the torque error. In TC-VS, torque control is performed indirectly using a velocity servo interface of an electric motor; hence, the torque error is somehow accommodated in the desired velocity. In fact, through the interpretation of the torque control problem as a deflection control of the elastic element, it is also possible to perform torque control via position servo (TC-PS) [20]–[22]. However, TC-PS approaches can be merged into the TC-DF category, because control of spring deflection and that of spring torque are equivalent.

TC-DF approaches mainly focus on applying robust control techniques to torque dynamics to achieve robust performance of $\tau_j \to \tau_d$ tracking [18]–[21], [23]. However, despite many success stories, TC-DF approaches are commonly limited by the fact that the acceleration signal is amplified by the D-gains of torque tracking and impedance controllers, while D-control is required to ensure stability. Because the amplified discrepancy occurring in the acceleration calculations may degrade the control performance, the achievable control gains might be limited. This limitation is especially true for applications associated with highly dynamic motions, which make acceleration calculations untrustworthy. In this regard, [24], [25] reported trade-offs between achievable control gains and robustness.

TC-VS approaches [1], [16], [26], [27] allow us to avoid an explicit D-control term. Due to the absence of the D-term, TC-VS might be a suitable choice for the applications associated with highly dynamic motions. For example, a group proposed a TC-DF [18] for robot arm control used TC-VS for bipedal walking, which involves periodic collisions with the ground [28]. However, TC-VS is also limited in that it does not guarantee the passivity of the link-side impedance controller when the SEA is an ideal viscous-free element [29]. This sounds somewhat contradictory because the 'ideal' design of the SEA eliminates the passivity property.

To summarize, although SEA TC-DF can achieve passivity in theory, it may not be successful in practice because of the interference of the acceleration amplification with the control gains.

C. Passivity of FJR with inner-loop SEA torque control

Again, it is hard to consider the SEA as a pure torque source due to the dynamics of the motor-side inertia. Consequently, the passivity of the link-side impedance control is not trivial even if the inner-loop torque dynamics themselves are stable. Passivation techniques such as time domain passivity control can be used to ensure the passivity of the impedance control [27]. However, this paper aims at achieving passivity without relying on passivation techniques that recover passivity by sacrificing the control performance when the passivity condition is violated.

Several studies have performed passivity analysis of SEA TC-DF [15], [25], [30]. Conditions for passivity could be obtained by investigating the resulting transfer function from $\dot{q}$ to τ_j. Another pioneering study [16] showed that the passivity of SEA TC-VS can be satisfied if a certain gain condition is met. In this study, however, TC-VS was modified to have an explicit D-control term, because the original TC-VS (which lacks the D-term) does not guarantee passivity [29]. Again, the D-term may cause a limitation due to the amplification of the acceleration signals.

Interestingly, [31] experimentally validated the passivity of the original TC-VS by investigating the resulting Bode plot. In fact, this result was due to the non-negligible viscous effect of the joint, which motivates us to include it in the modeling and analysis.

D. Adding viscous element to the joints

In practice, it is not possible to completely avoid the viscous effect in a robot joint. Nevertheless, apart from a few exceptions (e.g., [32]), this effect is typically regarded as harmful and should be reduced as much as possible, and consequently, it is often omitted in the modeling and analysis. It should be mentioned that the viscous element is different from the joint friction, which is usually modeled only on the motor-side dynamics mainly due to the gear transmission. In

[1]However, in general, passivity does not imply stability, and vice versa

contrast, the viscous element generates $D_j(\dot{\theta} - \dot{q})$ on both the motor and link inertias, as shown in Fig. 2.

In some studies, including this paper, the joint viscosity is added intentionally by several means. For instance, [32] employed a piezoelectric actuator to utilize its properties such as being light weight and small in size. One recent study [33] proposed a viscoelastic actuator with an elastomer material that enables compact design by simplifying the drivetrains. However, elastomer elements are known to have hysteresis, which the designer should pay attention to. In contrast, we employed a spring-damper element utilizing an elastic spring element in parallel with a viscous damper. By doing so, our SvEA exhibits almost linear characteristics but at the cost of a bulkier design. Since the mechanical design of SvEA is beyond the scope of this paper, a dedicated article on that topic is currently in preparation.

The fundamental properties of SvEA are well studied in [32]. In [32], it is shown that the SvEA can perform well in terms of dynamic performance (maximum achievable link speed) and energy efficiency when the operating range is outside of the resonance frequency. This might be surprising because joint viscosity is often considered as an energy dissipating element. However, higher dynamic performance and energy efficiency can be achieved at the cost of safety due to the increased joint rigidity. In addition, [34] mathematically showed that the viscous element increases the torque control bandwidth.

Actually, the viscous element strengthens the coupling between the motor and link inertia, whereas the SEA decouples them by a spring element. The characteristics of SvEA are somewhere in between those of a rigid joint and an SEA. This is mathematically clear when we investigate the transfer functions. For example, considering Fig. 2, the open-loop transfer function of the external torque to the motor acceleration is (D_l is omitted for simplicity):

$$\ddot{\theta}(s) = \frac{D_j s + K_j}{BMs^2 + D_j(M+B)s + K_j(M+B)} \tau_{ext}(s) \quad (1)$$

and that of the output impedance is

$$\tau_{ext}(s) = \frac{BMs^3 + D_j(M+B)s^2 + K_j(M+B)s}{Bs^2 + D_j s + K_j} \dot{q}(s). \quad (2)$$

Magnitude Bode plots with varying D_j are shown in Fig. 3, and it is clear that the SvEA is somewhere between a rigid joint and an SEA depending on the value of D_j. Indeed, (1) and (2) become the transfer functions of a rigid joint as $D_j \to \infty$ and become those of an SEA when $D_j = 0$.

Naturally, variable designs are also studied to span a wide range of the system characteristics [35], [36]. In fact, our system is also variable, but this will not be discussed because it is beyond the scope of this paper. How to take advantage of the variability is one of our future topics to address. No matter which setup is chosen (variable or fixed), an intentional viscous element is used mainly to damp out the link-side motion [36] but not used for joint torque control applications.

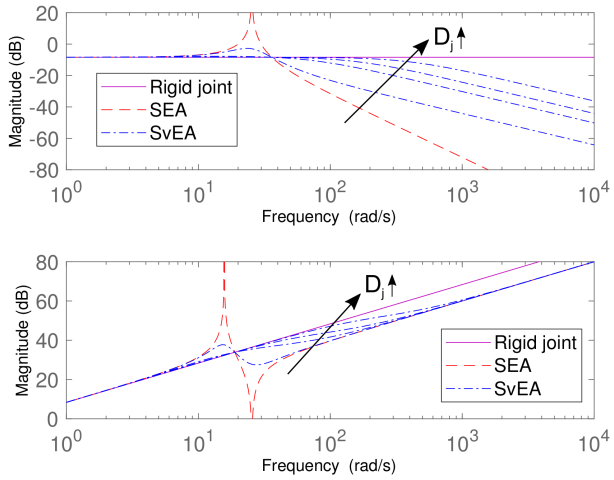

Fig. 3. Top: magnitude Bode plot for (1). Bottom: the plot for (2). An SvEA behaves like an SEA when D_j is small and behaves like a rigid joint as D_j increases. This is physically understandable because a large D_j makes the joint coupling stronger.

E. Contributions of this paper

This paper proposes a generic control structure that leads to a passivity and stability analysis of SEA/SvEA-based FJRs. In particular, we derive sufficient conditions that theoretically guarantee passivity and stability. We find that only SvEA has potential to truely achieve the sufficient conditions.

More specifically, the analysis of an SEA case may become invalid in practice due to acceleration amplification mentioned earlier, and consequently, the achievable control gains of torque controllers are limited in practice. In contrast, the use of an SvEA significantly reduces the amount of acceleration amplification, because the acceleration signals are not amplified by control gains. This implies that the theoretical analysis of an SvEA is valid in real implementations. As a result, link-side impedance controllers can be realized without limiting the control gains of inner-loop torque controller. We would like to underline that the reduction of acceleration amplification itself is not the main goal of the paper, but is a mean to realize link-side impedance controller more robustly.

In addition, we remark a couple of theoretical advances. First, the framework proposed in this paper extends passivity analysis to nonlinear FJRs (Theorem 1), where conventional analyses are limited to linear systems. In this paper, standard forms of TC-DF and TC-VS of both SEA and SvEA are analyzed with nonlinear link-side dynamics. Second, our analysis shows that many of existing passivity analyses (performed without considering the gravity term) turn out to be sufficient in the sense that they can fit into the proposed framework with little modification (Remark 3).

An important message of this paper is that the joint viscosity, which is typically minimized as much as possible from the design stage, might be beneficial for torque control problems. Therefore, one should take joint viscosity into account in the hardware design, modeling, and analysis.

Part of this paper was presented in [37]. More specifically,

[37] focused on the fact that the SvEA torque control does not require D-control. The passivity and stability analysis of the entire control loop is a new contribution of this paper.

F. Organization of the paper

Section II presents modeling of SEA and SvEA-based FJRs with inner-loop torque control designs. Section III proposes a generic framework that leads us to the stability and passivity analysis of the overall dynamics (inner-loop as well as outer-loop). Section IV derives sufficient gains conditions using the proposed framework. Section V presents simulation and experimental validations, and Section VI concludes the paper.

II. Modeling and Control of SEA/SvEA-based FJR

This section presents torque control methods for SEA and SvEA, focusing only on the inner-loop torque dynamics. Stability and passivity analysis of the entire FJR system is presented in next section.

A. FJR dynamics

A schematic diagram of an SEA- or SvEA-based system is shown in Fig. 2. The equation of motion of an FJR is given by[2]

$$M(q)\ddot{q} + (C(q,\dot{q}) + D_l)\,\dot{q} = \tau_j - \tau_g(q) + \tau_{ext}, \tag{3}$$

$$B\ddot{\theta} + \tau_j = \tau_m, \tag{4}$$

$$\tau_j = K_j(\theta - q) + D_j(\dot{\theta} - \dot{q}), \tag{5}$$

where the diagonal matrix B represents the motor-side inertia, M, C, τ_g represent the link-side inertia, Coriolis/centrifugal, and gravity matrices/vector, respectively. $D_l > 0$ represents the link-side viscous friction. θ and q are the motor and link side positions, and τ_m, τ_j, and τ_{ext} are the motor torque, joint torque, and external torque, respectively. K_j and D_j are diagonal matrices representing joint stiffness and viscosity. In a typical elastic joint setup, τ_j can be observed either by a sensor or system states, but τ_{ext} is usually unknown.

In representing an FJR (3)-(4), one of the typical choices for the system state is q, $\dot{q}$, θ, and $\dot{\theta}$. In this paper, however, the system is represented using τ_j and $\dot{\tau}_j$ instead of θ and $\dot{\theta}$ because τ_j is the control variable. Therefore, θ is replaced by τ_j and q using $\theta = K_j^{-1}\tau_j + q$ for SEA, and $\theta = (D_j s + K_j)^{-1}\tau_j + q$ for SvEA.[3]

This paper aims at controlling the link-side dynamics (3) by making the joint torque τ_j follow a user-defined desired joint torque τ_d. As a link-side controller, the following impedance control realized by PD plus gravity compensation is of particular interest in this paper.

$$\tau_d = \underbrace{K_p(q_d - q) - K_d\dot{q}}_{=\tau_{pd}} + \tau_g, \tag{6}$$

where K_p and K_d are diagonal matrices representing PD gains, and q_d means the desired value for q. For consistency with later sections, let us state the problem slightly differently: The control objective is to make $\tau_j - \tau_g$ follow τ_{pd}, so (3) is shaped into

$$M(q)\ddot{q} + (C(q,\dot{q}) + D_l + K_d)\,\dot{q} + K_p(q - q_d) = \tau_{ext}. \tag{7}$$

B. SEA TC-DF

Consider the torque generated by SEA ($D_j = 0$ in (5)):

$$\tau_j = K_j(\theta - q). \tag{8}$$

As stated earlier, the control goal is to make $\tau_j - \tau_g$ follow τ_{pd}. Therefore, let us define an output variable as $y = \tau_j - \tau_g$, instead of $y = \tau_j$. The SEA torque dynamics are obtained by taking double derivative of y:

$$\begin{aligned}\ddot{\tau}_j - \ddot{\tau}_g =& K_j(\ddot{\theta} - \ddot{q}) - \ddot{\tau}_g \\ =& K_j(B^{-1}(\tau_m - \tau_j) - \ddot{q}) - \ddot{\tau}_g.\end{aligned} \tag{9}$$

Consider a control law

$$\tau_m = \tau_j + B\ddot{q} + BK_j^{-1}\ddot{\tau}_g + Bu, \tag{10}$$

where u is a new control input. Then, (9) reduces to the following linearized output dynamics:

$$\ddot{\tau}_j - \ddot{\tau}_g = K_j u. \tag{11}$$

From the spirit of the cascade control structure, the torque dynamics have to be stable. While PD is sufficient for stability, PID is employed in this paper for more generality:

$$u = L_d\dot{e}_\tau + L_p e_\tau + L_i \int e_\tau, \tag{12}$$

where $L_p, L_d, L_i > 0$ are constant diagonal gain matrices and $e_\tau = \tau_d - \tau_j$ is the torque error. Since e_τ can be alternatively represented as $e_\tau = \tau_{pd} - (\tau_j - \tau_g)$, the resulting closed-loop dynamics can be represented using a transfer function as

$$\begin{aligned}&\tau_j(s) - \tau_g(s) = \\ &\left(K_j^{-1}s^3 + L_d s^2 + L_p s + L_i\right)^{-1}\left(L_d s^2 + L_p s + L_i\right)\tau_{pd}(s).\end{aligned} \tag{13}$$

The right hand side represents the low pass filter of $\tau_{pd}(s)$. The stability of (13) can be easily checked by investigating the poles.

C. SvEA TC-DF

The torque generated by SvEA is given by (5), which is $\tau_j = K_j(\theta - q) + D_j(\dot{\theta} - \dot{q})$. SvEA torque dynamics are obtained by taking a time derivative of the output $y = \tau_j - \tau_g$:

$$\begin{aligned}\dot{\tau}_j =& K_j(\dot{\theta} - \dot{q}) + D_j(\ddot{\theta} - \ddot{q}) \\ =& K_j(\dot{\theta} - \dot{q}) + D_j(B^{-1}(\tau_m - \tau_j) - \ddot{q}).\end{aligned} \tag{14}$$

Compared to (9), the order of the torque dynamics is reduced by one.

Remark 1 (Internal dynamics of SvEA joint torque control)**.** *The elastic joint system has 4th order dynamics. For example,*

[2]To be precise, inertial coupling between the motor- and link-side inertia may be present in general [38]. However, the coupling is often negligible in practice.

[3]Throughout the paper, an abuse of notation is allowed for s, assuming that relevant matrices are diagonal.

in the SEA case, 4th order dynamics can be represented using q, $\dot{q}$, τ_j, and $\dot{\tau}_j$ (or $\tau_j - \tau_g$ and its derivative) because the torque dynamics have an order of two. However, those of SvEA have an order of one, so internal dynamics of an order of one exist, which are represented by $K_j\delta + D_j\dot{\delta} = \tau_j$ with $\delta = \theta - q$. As long as the joint torque tracking is stable, the internal dynamics are also stable. Therefore, the internal dynamics are not considered in the following.

For control design purposes, we take one more time derivative of (14):

$$\begin{aligned}\ddot{\tau}_j - \ddot{\tau}_g =& K_j(B^{-1}(\tau_m - \tau_j) - \ddot{q}) \\ &+ D_j(B^{-1}(\dot{\tau}_m - \dot{\tau}_j) - \dddot{q}) - \ddot{\tau}_g. \end{aligned} \tag{15}$$

Similar to the SEA TC-DF case, let us apply feedback linearization using a control law given by

$$\tau_m = \tau_j + B\ddot{q} + (D_j s + K_j)^{-1} B\ddot{\tau}_g + Bu. \tag{16}$$

Then, (15) becomes

$$\ddot{\tau}_j - \ddot{\tau}_g = D_j\dot{u} + K_j u. \tag{17}$$

The torque dynamics (17) can be stabilized by the following PI torque control because $\dot{u}$ produces derivative feedback from the P-control term.

$$u = L_p e_\tau + L_i \int e_\tau. \tag{18}$$

Then, the closed-loop torque dynamics become

$$\begin{aligned}&\tau_j(s) - \tau_g(s) \\ &= \left(s^3 + D_j L_p s^2 + (K_j L_p + D_j L_i)s + K_j L_i\right)^{-1} \times \\ &\quad \left(D_j L_p s^2 + (K_j L_p + D_j L_i)s + K_j L_i\right) \tau_{pd}(s). \end{aligned} \tag{19}$$

Again, the stability can be easily checked by investigating the poles.

III. A Framework for Stability and Passivity Analysis of FJR Impedance Controllers

In the previous section, SEA and SvEA inner-loop torque control methods are introduced to realize link-side impedance behavior (7). If τ_d is perfectly realized, the stability and passivity of the FJR are straightforward. However, due to the nonnegligible torque dynamics, τ_d cannot be realized exactly, and therefore, a more elaborate analysis is needed. In this section, we devise a generic framework to ensure the stability and passivity of both SEA- and SvEA-based FJRs.

A. Passivity-based analysis for environmental interaction

Before introducing theoretical treatments, this subsection addresses the context in which this paper deals with passivity. Fig. 5 shows an illustrative example that is used throughout the paper. Consider a single link FJR that interacts with a passive environment that can be modeled using a spring. Imagine that a link that is driven into the environment by the PD impedance controller (Fig. 5a) bounces on this environment. If the impedance behavior is perfectly realized, it is physically clear that energy can only be dissipated during the collision, and the height of the link after each bounce decreases. As

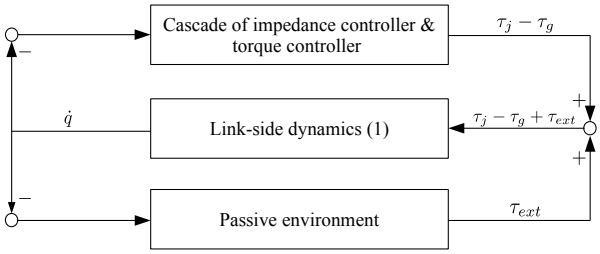

Fig. 4. Rearrangement of Fig. 1 for passivity-based analysis of the FJR with inner-loop torque controllers. If the torque controller is designed to satisfy the passivity of the I/O pair $(-\dot{q}, \tau_j - \tau_g)$, the overall control loop is constructed by feedback interconnections of passive systems. As a result, energy is not generated inside the closed-loop.

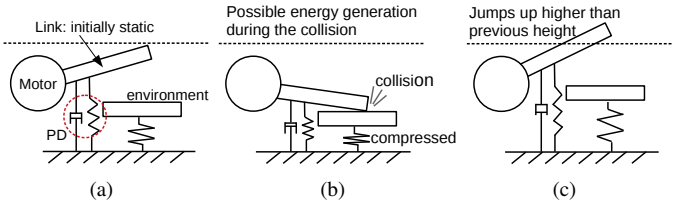

Fig. 5. An illustrative example of possible energy generation during collision with an environment. Passivity guarantees that energy is not generated during the collision, and therefore, the height of each bounce can only decrease.

addressed in the previous section, the impedance behavior is realized by a cascaded torque controller, which has its own dynamics, as addressed in the previous section. Therefore, there is a chance of energy generation during the collision (Fig. 5b), and as a result, the link may jump higher than the initial position (Fig. 5c).

Passivity provides a systematic approach for energy-based analysis. Although the passivity properties of FJRs with torque controlled SEAs have been studied in the literature, the analyses were limited to gravity-free single-link systems because the transfer function methods were the main tool. This paper employs another method that can be scaled to general nonlinear systems: feedback interconnection of passive systems preserves passivity. Based on this fact, this paper aims at establishing the control structure shown in Fig. 4. In the figure, we remark that the output of the control block is $\tau_j - \tau_g$, not τ_j. This is a trick to handle the gravity term τ_g, which is the most unmanageable term in the passivity analysis of FJRs.

It is well known that the link-side multibody dynamics are output strictly passive. The environment is also passive because it can be modeled by a spring. If the I/O pair $(-\dot{q}, \tau_j - \tau_g)$ of the control block is also passive, then the entire control loop is constructed by feedback interconnections of passive systems. This indicates that the robot never generates energy during environmental interactions. Therefore, the main challenge from the passivity perspective is to determine the passivity of the controller's I/O pair $(-\dot{q}, \tau_j - \tau_g)$.

B. Preliminary: conditional stability

Passivity is often associated with a storage function that is required to be positive semidefinite. Due to the lack of positive definiteness, in general, passivity does not guarantee stability. Fortunately, stability can be claimed from passivity

when some conditions are properly combined. In particular, this paper employs so-called conditional stability, which is a weaker version of Lyapunov stability. When it is combined with passivity, the term 'conditional' can be dropped, and the usual Lyapunov stability can be claimed. For the sake of completeness, we summarize the relevant preliminary below.

Consider an autonomous system

$$\dot{z} = f(z) \tag{20}$$

with $z \in \Re^n$. Assume again that z^* is an equilibrium point satisfying $f(z^*) = 0$. Suppose that (20) has a solution for initial state $z(0) = z_0 \ \forall t > 0$.

Definition 1. *[39] An equilibrium point $z^* \in \mathcal{A}$ of (20) is said to be*

1) *stable conditional to the set $\mathcal{A}$ if for any $\epsilon > 0$, there exists a $\delta > 0$ such that the following can be satisfied for any $z_0 \in \mathcal{A}$:*

$$||z_0 - z^*|| < \delta \Rightarrow ||z(t) - z^*|| < \epsilon, \ \ \forall t \geq 0. \tag{21}$$

2) *asymptotically stable conditional to $\mathcal{A}$ if the point is stable and there exists an $\eta > 0$ such that the following can be satisfied for any $z_0 \in \mathcal{A}$:*

$$||z_o - z^*|| < \eta \Rightarrow \lim_{t\to\infty} z(t) = z^*. \tag{22}$$

The definition of conditional stability states that all requirements of Lyapunov stability must hold only for the initial conditions in a particular set; i.e., $z_0 \in \mathcal{A} \subset \Re^n$. Therefore, Lyapunov stability is stronger than conditional stability.

The following lemma allows us to conclude asymptotic stability (in the sense of Lyapunov) from conditional stability.

Lemma 1. *[40] Consider a system*

$$\dot{z} = f(z) + g(z)v, \tag{23}$$
$$y = h(z), \tag{24}$$

where $z \in \Re^n$, $v \in \Re^m$, and $y \in \Re^m$ are the state, input, and output, respectively. Let $\mathcal{A}$ be the largest positively invariant set contained in $\{z|h(z) = 0\}$. Suppose this system satisfies output strict passivity. If the equilibrium is asymptotically stable conditional to $\mathcal{A}$, then it is asymptotically stable when $v = 0$.

C. A generic framework

Fig. 6 shows a generic control framework that leads us to the stability and passivity analysis of SEA/SvEA-based FJRs in a unified way. One unique feature of Fig. 6 is that the output of the torque control is $\tau_j - \tau_g$, not τ_j. Through this, the cascade of impedance control and torque control can be interconnected with the link-side dynamics (which are inherently passive) by feedback that preserves passivity.

The framework can be applied when the torque controller allows to represent red box in Fig. 6 as a transfer function $\frac{\tau_j - \tau_g}{\tau_{pd}}(s)$. Table I summarizes how the SEA TC-DF and SvEA TC-DF presented in the previous section fit into the framework. Then, the analysis can be performed using the following theorem.

Theorem 1. *Consider the control structure shown in Fig. 6. If (i) there exists a unique equilibrium point, (ii) the transfer function from $-\dot{q}$ to $\tau_j - \tau_g$ is positive real and (iii) the system is asymptotically stable conditional to $\dot{q} = 0$, then*

- *the equilibrium of the closed-loop system is asymptotically stable when $\tau_{ext} = 0$;*
- *the I/O pair $(\tau_{ext}, \dot{q})$ is passive when $\tau_{ext} \neq 0$.*

Proof. Since the transfer function from $-\dot{q}$ to $\tau_j - \tau_g$ is positive real, there exists a storage function $S(x)$ that satisfies $\dot{S}(x) \leq -\dot{q}^T(\tau_j - \tau_g)$, where x is a state associated with the transfer function. This is a well-known result from the positive real lemma [41]. Then, $V(x, q, \dot{q}) = S(x) + \frac{1}{2}\dot{q}^T M(q)\dot{q} \geq 0$ can be used as a storage function for the overall dynamics. The I/O pair $(\tau_{ext}, \dot{q})$ is output strictly passive because $\dot{V} \leq \dot{q}^T\tau_{ext} - \dot{q}^T D_l \dot{q}$. Moreover, by combining the passivity (which was just proven) with conditional stability (requirement (iii) of this theorem), Lemma 1 allows us to drop 'conditionally to $\dot{q}$' and conclude asymptotic stability. □

For our system, requirement (iii) is satisfied if the reduced system obtained by letting $\dot{q} = 0$ is asymptotically stable. When conditional stability is combined with requirement (ii), we can conclude asymptotic stability in the sense of Lyapunov. Notice that, in this paper, the desired PD gains K_p and K_d have to be diagonal, because Fig. 6 requires to express the PD controller as a transfer function $(K_d s + K_p)/s$.

IV. Derivation of Sufficient Conditions for Stability and Passivity

A. Sufficient conditions for SEA TC-DF and limitations

Although stable torque tracking can be achieved in the sense of (13),[4] passivity and stability of the entire system are not trivial. The following theorem presents sufficient gain conditions by applying Theorem 1.

Theorem 2. *Consider SEA TC-DF (10) with (12). If the control gains are chosen to satisfy*

$$K_j L_d L_p - L_i > 0, \tag{25}$$
$$K_j K_d L_d^2 - (K_d L_p + K_p L_d) > 0, \tag{26}$$
$$K_j K_d L_p^2 + K_p L_i - 2K_j K_d L_d L_i > 0, \tag{27}$$

then the I/O pair $(\tau_{ext}, \dot{q})$ is passive and the unique equilibrium point of system is asymptotically stable when $\tau_{ext} = 0$.

Proof. To begin with, notice that it can be easily checked that there exists a unique equilibrium point for the system; $q = q_d$, $\tau_j - \tau_g = 0$ with zero derivatives. Next, to apply Theorem 1, let us show asymptotic stability conditional to $\dot{q} = 0$. Because $\dot{q} = 0$ implies $\tau_j - \tau_g = 0$ from the link-side dynamics, we can further state that

$$e_\tau = K_p(q_d - q), \ \dot{e}_\tau = 0, \text{ and } \ddot{e}_\tau = 0 \tag{28}$$

[4]To avoid confusion, asymptotically (or exponentially) stable torque tracking is not achieved. To achieve asymptotically/exponentially stable torque tracking, $\ddot{\tau}_{pd}$, which may include the amplified jerk ($\dddot{q}$) term, should be included in the control law.

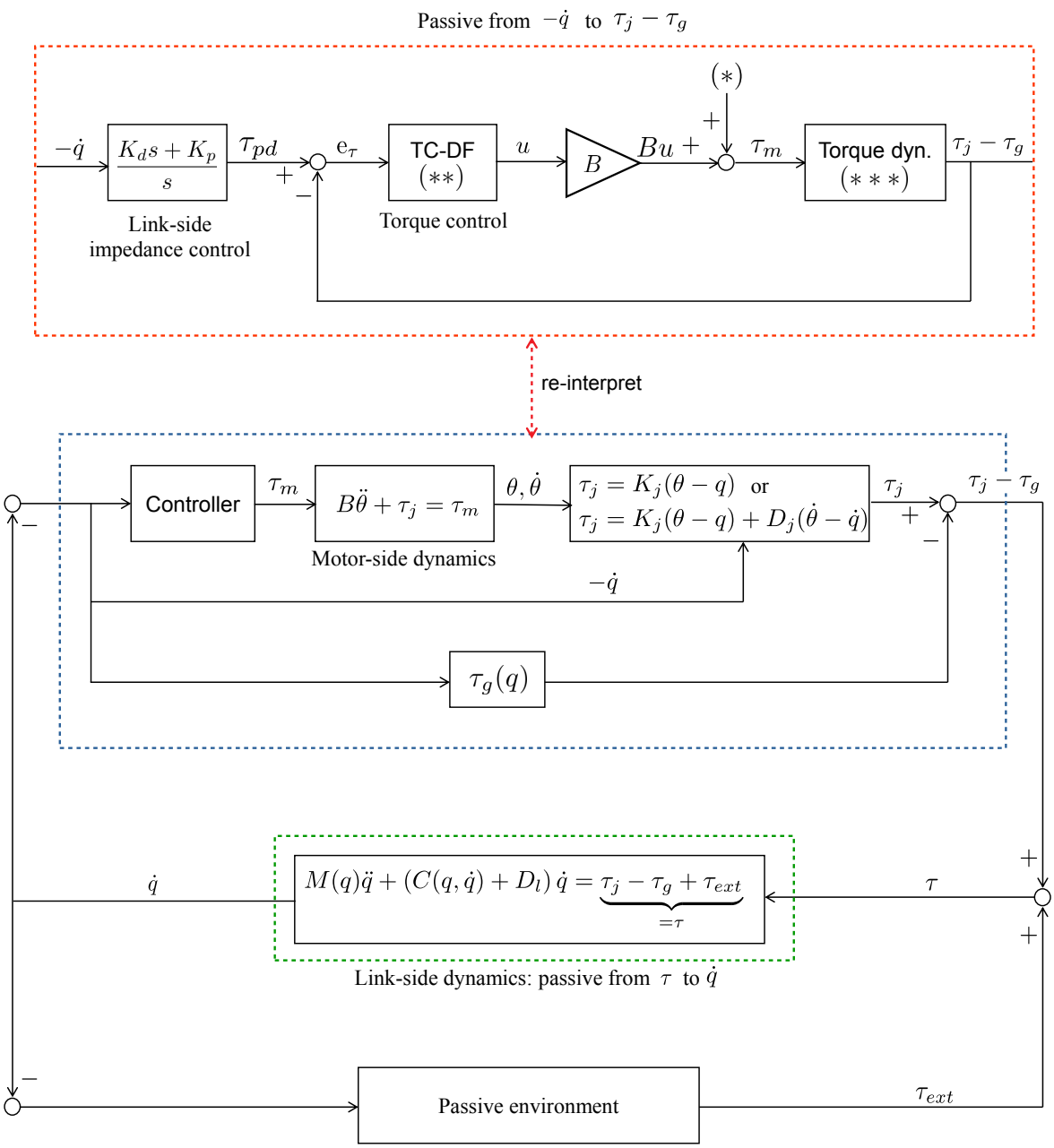

Fig. 6. A generic control structure. The control structure with original robot dynamics (3)-(5) is shown using the blue and green dotted boxes. With the control laws τ_m proposed in this paper, the blue box can be interpreted as the scheme boxed with a red dotted line. If the passivity of the I/O pair $(-\dot{q}, \tau_j - \tau_g)$ in the red dotted box can be shown, the overall control structure is then constructed by feedback interconnections of passive subsystems. Therefore, there is no energy generation in the closed-loop. Expressions for $(*)$, $(**)$, $(***)$, and the resulting τ_m are summarized in Table I. Moreover, the transfer function $\frac{\tau_j - \tau_g}{\tau_{pd}}(s)$ is shown in the table. The transfer function from $-\dot{q}$ to $\tau_j - \tau_g$ (which is needed for passivity analysis) is simply $\frac{K_d s + K_p}{s} \cdot \frac{\tau_j - \tau_g}{\tau_{pd}}(s)$.

TABLE I

	(*)	(**)	Resulting τ_m	(***)	$\frac{\tau_j - \tau_g}{\tau_{pd}}(s)$
SEA TC-DF	$\tau_j + B\ddot{q} + BK_j^{-1}\ddot{\tau}_g$	PID in (12)	(10)	(9)	(13)
SvEA TC-DF	$\tau_j + B\ddot{q} + (D_j s + K_j)^{-1} B\ddot{\tau}_g$	PI in (18)	(16)	(15)	(19)

since $e_\tau = \tau_{pd} + \tau_g - \tau_j = \tau_{pd} = K_p(q_d - q) - K_d\dot{q} = K_p(q_d - q)$. Then, we can rewrite (11)-(12) as

$$\ddot{e}_\tau + L_d\dot{e}_\tau + L_p e_\tau + L_i \int e_\tau = \ddot{\tau}_{pd} = 0, \tag{29}$$

which can be further expressed as

$$L_p(q_d - q) + L_i \int (q_d - q) = 0, \tag{30}$$

using (28). Therefore, asymptotic stability conditional to $\dot{q} = 0$ can be concluded because (30) is asymptotically stable.

Next, let us show that the transfer function from $-\dot{q}$ to $\tau_j - \tau_g$ given below is positive real.

$$\begin{aligned}\frac{\tau_j - \tau_g}{-\dot{q}} =& s^{-1}\left(K_j^{-1}s^3 + L_d s^2 + L_p s + L_i\right)^{-1} \times \\ & (K_d s + K_p)(L_d s^2 + L_p s + L_i).\end{aligned} \tag{31}$$

To this end, we have to show that (i) (31) is stable and (ii) the real part of (31) with $s = jw$ is positive for all $w > 0$.

For (i), the Routh Hurwitz criterion requires that $L_d, L_p, L_i > 0$ and $L_d L_p > K_j^{-1} L_i$. For (ii), the real part can be obtained as

$$\mathbb{R}\left(\frac{\tau_j - \tau_g}{-\dot{q}}(jw)\right) = \frac{1}{den}\left(a_6 w^6 + a_4 w^4 + a_2 w^2\right), \tag{32}$$

where den is some positive constant. The coefficients are

$$a_6 = K_j K_d L_d^2 - K_d L_p - K_p L_d, \tag{33}$$

$$a_4 = K_j K_d L_p^2 + K_p L_i - 2K_j K_d L_d L_i, \tag{34}$$

$$a_2 = K_j K_d L_i^2. \tag{35}$$

A sufficient condition to guarantee (32)>0 for all $w > 0$ is $a_6, a_4 > 0$.

Combining all these, we arrive at conditions (25)-(27), under which both requirements of Theorem 1 are satisfied. Consequently, stability and passivity can be claimed. □

This theorem derived sufficient conditions (25)-(27) for stability and passivity of the FJR with SEA TC-DF. However, one limitation is the fact that D-control is needed ($L_d > 0$) to satisfy the conditions. More specifically, the D-control law $L_d(\dot{\tau}_d - \dot{\tau}_j)$ may be problematic because it amplifies the acceleration signal by the control gains L_d and K_d:

$$L_d\dot{\tau}_d = L_d(-K_p\dot{q} - K_d\ddot{q}). \tag{36}$$

In practice, reliable calculation of the acceleration is very difficult mainly because of quantization noise, especially when the measurement frequency is high. Low-pass filters are often utilized to cope with the differentiation noise, but they introduce phase delay, which again implies a discrepancy that should not be amplified. Notably, there are some efforts to extract acceleration information more reliably, e.g., [42]. However, amplified acceleration feedback, especially that with large gains, is something that requires further research to be used in the controller. As a result, the validity of the theoretical analysis is jeopardized in real implementations. Indeed, in Section V, we show that there is a trade-off between achievable control gains and robustness, especially when highly dynamic motions such as collisions are involved.

As a digression, one may use a TC-VS approach to alleviate the limitation associated with acceleration amplification:

$$\tau_m = PI(\dot{\theta}_d - \dot{\theta}) \tag{37}$$

with

$$\dot{\theta}_d = PI(\tau_d - \tau_j). \tag{38}$$

Note that $\dot{\theta}$ in (37) implicitly generates a $\dot{\tau}_j$ component because $\dot{\theta} = K_j^{-1}\dot{\tau}_j + \dot{q}$. Therefore, the D-control law is no longer needed from a stability point of view. However, as studied in [29], passivity cannot be satisfied because the relative order between $\dot{q}$ and τ_j is two even for the linear case.[5]

Remark 2. *In this paper, a PID-type TC-DF (12) is considered, while PD-types are also frequently used in literature. The passivity/stability condition for a PD-type TC-DF can be obtained by simply letting $L_i = 0$ in (25)-(27).*

Remark 3. *Any controllers satisfying passivity of the I/O pair $(\dot{q}, \tau_j)$ can be extended to satisfy that of $(\dot{q}, \tau_j - \tau_g)$. Assume that a controller $\tau_m = v$ is designed to satisfy passivity of the I/O pair $(\dot{q}, \tau_j)$. Then, letting $\tau_m = v + BK_j^{-1}\ddot{\tau}_g$ as a new control input, the I/O pair $(\dot{q}, \tau_j - \tau_g)$ becomes passive. Therefore, the passivity analysis performed without considering gravity (e.g., [16], [29]) is sufficient in the sense that gravity can be easily included with little modification.*

B. Sufficient conditions for SvEA TC-DF

The following theorem derives sufficient gain conditions for stability and passivity of SvEA TC-DF.

Theorem 3. *Consider the SvEA TC-DF in (16) and (18). If the control gains are chosen to satisfy*

$$D_j^2 K_d L_p^2 - (D_j K_p + K_j K_d)L_p - D_j K_d L_i > 0, \tag{39}$$

then the I/O pair $(\tau_{ext}, \dot{q})$ is passive, and the unique equilibrium point of system is asymptotically stable when $\tau_{ext} = 0$.

Proof. The first part of the proof is similar to that of Theorem 2. The real part of the transfer function is given by

$$\mathbb{R}\left(\frac{\tau_j - \tau_g}{-\dot{q}}(jw)\right) = \frac{1}{den}\left(a_4 w^4 + a_2 w^2\right), \tag{40}$$

where den is some positive constant. The coefficients are

$$a_4 = D_j^2 K_d L_p^2 - (D_j K_p + K_j K_d)L_p - D_j K_d L_i, \tag{41}$$

$$a_2 = K_d L_i^2. \tag{42}$$

A sufficient condition to guarantee (40)>0 for all $w > 0$ is $a_4 > 0$, which is given in (39). □

Notice that, unlike the SEA case, the SvEA TC-DF shown in (16) and (18) does not require to have the D-control term. Therefore, the above theorem implies that the stability and

[5]To meet the passivity condition, the maximum allowable phase delay is ± 90. This means that the relative order of a transfer function of interest should be ≤ 1 (as a necessary condition), because the terminal phase is determined by the relative orders. However, by substituting (37) into (9) together with (38) and $\tau_d = PI(\dot{q})$, the resulting relative order of the transfer function from $\dot{q}$ to τ_j is two. Therefore, the necessary condition is violated.

passivity are satisfied without amplification of the acceleration feedback with the control gains. In Section V, we show that the theoretical analysis (i.e., (39)) is valid in real implementations.

Remark 4. *In contrast to the SEA case, SvEA TC-VS can be implemented while preserving passivity. Consider a velocity PI control*

$$\tau_m = P_w(\dot{\theta}_d - \dot{\theta}) + I_w(\theta_d - \theta). \tag{43}$$

Define the desired velocity $\dot{\theta}_d$ by

$$\dot{\theta}_d = \dot{\theta} + BL_p e_\tau + (I_w s + P_w)^{-1} s \left(B\ddot{q} + \tau_j + (D_j s + K_j)^{-1} B\ddot{\tau}_g \right). \tag{44}$$

Substituting (43)-(44) into (15), the closed-loop torque dynamics are

$$\ddot{\tau}_j - \ddot{\tau}_g = L_p \left(D_j P_w \dot{e}_\tau + (K_j P_w + D_j I_w) e_\tau + K_j I_w \int e_\tau \right), \tag{45}$$

which are similar to those for the SvEA TC-DF case. As a result, it can be said that TC-DF is realized via the electric motor's velocity servo interface instead of the torque interface.

C. Discussion on feedback linearizing actions

The torque control laws are designed together with feedback linearization actions that include (i) the cancellation of $B\ddot{q}$ and (ii) gravity-related terms: see (10) and (16). Let us investigate each in the following.

1) Cancellation of $B\ddot{q}$: $B\ddot{q}$ cancellation is included to cancel out the nonlinear dynamics in the analysis. Moreover, some studies have shown that link-velocity/acceleration terms should be eliminated to achieve a high performance torque controller. This is sometimes called load motion compensation [43]. Notably, [44] reported that instability is possible when $B\ddot{q}$ is overcompensated. Therefore, one should be careful not to overcompensate it in a real implementation. Incomplete compensation of $B\ddot{q}$ may result in energy generation, which counteracts passivity. In fact, there are other unmodeled factors (e.g., time delays and the dynamics of low-pass filters) that may also threaten passivity. To alleviate these concerns, in practice, the control gains should be selected to have large enough margins in conditions (25)-(27) or (39). One may refer to a recent study [45] for a more elaborate analysis on $B\ddot{q}$ compensation.

In addition, $B\ddot{q}$ results in feedback of noisy signals, especially when the value of B is large due to the reduction gears. Nevertheless, in our experience, the magnitude of B is typically far lower than that of the amplification due to the control gains. As is shown in Section V, the value of the motor inertia was $B = 1.62$ (with 1:100 gear transmission) and that of the acceleration-amplifying control gain was $L_d K_d \simeq 23$ in a simulation. In experiments, however, we had to reduce the gains to $K_d L_d \simeq 1.25$.

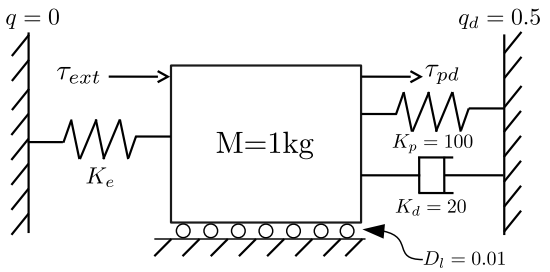

Fig. 7. Motivating example. Impedance controller τ_{pd} is realized on the link-side mass M using an inner-loop joint torque controller.

2) Gravity-related terms: $\ddot{\tau}_g$ related terms are included to make $\tau_j - \tau_g$ the output of the torque controller. In fact, [14], [46], and [47] also proposed control schemes that contain $\ddot{\tau}_g$ in the resulting control law but in different contexts. This paper presents a passivity perspective of having $\tau_j - \tau_g$ as an output; the overall control structure can be represented by feedback interconnections of passive subsystems, as shown in Fig. 4.

One limitation, however, is that the calculation of $\ddot{\tau}_g$ might be also noisy as it involves a double derivative. Fortunately, for our system, this quantity is divided by large values: $B\ddot{\tau}_g/(D_j s + K_j)$ for an SvEA and $B\ddot{\tau}_g/K_j$ for an SEA. Since K_j of our system is of an order of magnitude of $10^2 \mathrm{Nm/rad}$, the influence of the noise is strongly suppressed. Therefore, the $\ddot{\tau}_g$ term can even be neglected in implementations because the resulting value is sufficiently small. Nevertheless, we emphasize that this argument can be made only after formulating the full control law with $\tau_j - \tau_g$ as an output.

V. Simulation and Experimental Validations

Throughout the validation, the torque control gains are tuned using the following rules

$$\text{SEA: } L_d = \sigma^2/K_j,\ L_p = \sigma^3/K_j,\ L_i = \sigma^3/K_j, \tag{46}$$

$$\text{SvEA: } L_p = \sigma^2/D_j,\ L_i = \sigma^3/D_j. \tag{47}$$

where $\sigma > 0$ is a new control gain. With these tuning rules, the passivity/stability conditions ((25)-(27) for an SEA and (39) for an SvEA) are satisfied with a sufficiently large σ. Note that we are not trying to propose gain tuning rules. We made these rules to systematically tune multiple gains with a single parameter σ during the validation.

A. Validation of the theory with a simple example

The purpose of this subsection is to validate the theoretical findings. To this end, any unmodeled effects such as quantization, time-delay, and modeling uncertainty are neglected. In this section, we validate the sufficient conditions for an SvEA TC-DF (i.e., Theorem 3), which is the main interest of this paper. Comparison with an SEA TC-DF is shown in next section.

Consider a gravity-free SvEA system with $M = 1$ kg, $C = 0$, $D_l = 0.01$, $B = 1.62$ kg, $K_j = 400$ N/m, and $D_j = 10$ Ns/m. To realize the impedance behavior as described in Fig. 7, the PD law (6) is applied using TC-DF with $K_p = 100$ N/m, $K_d = 20$ Ns/m, and $\tau_g = 0$. Several parameter sets are considered as follows.

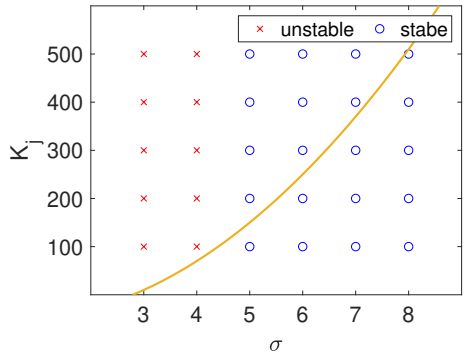

(a) $K_e = 100$

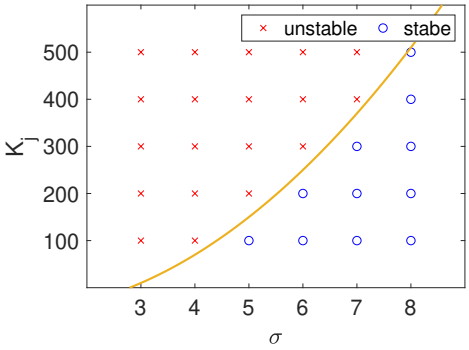

(b) $K_e = 10000$

Fig. 8. Stability for different combinations of K_j and σ with (a) $K_e = 100$ and (b) $K_e = 10000$. The right side of the orange curve satisfies passivity/stability condition (48), whereas the left side does not. For each combination of K_j and σ, 'o' ('x') indicates when the resulting response is stable (unstable).

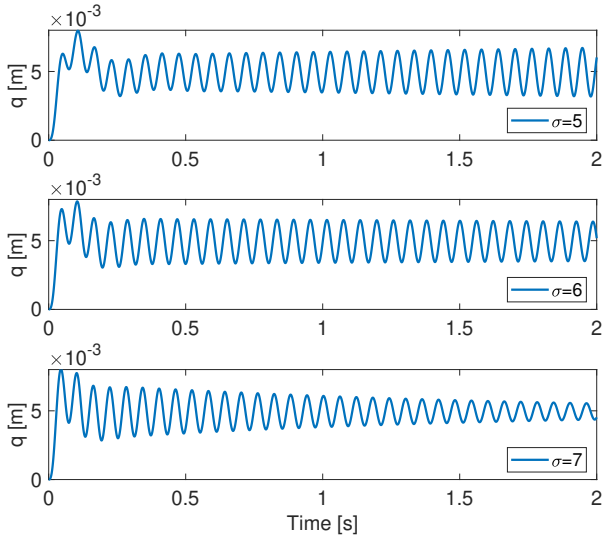

Fig. 9. To investigate the borderline cases, the responses for $\sigma = 5, 6, 7$ with $K_j = 200$ and $K_e = 10000$ are shown. According to (48), a stable response is expected for $\sigma > 5.5$. $\sigma = 5$ results in an unstable response which implies energy generation from the passivity perspective. $\sigma = 6$ results in a stable response but with very slow energy dissipation because the condition is barely met. $\sigma = 7$ shows faster energy dissipation.

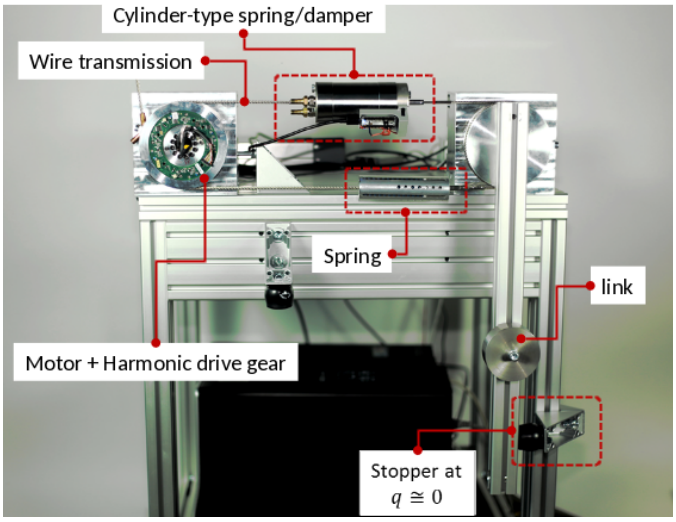

Fig. 10. Experimental setup. The left disc (motor-side) is connected by steel cables to the right disc (link-side). A joint of DLR LWR is used for the motor module (with a 1:100 gear ratio). The upper element generates viscous damping (to be precise, the cylinder also has a certain amount of stiffness), and the lower element contains a steel spring. An end-stop, which causes collisions in the experiments, is located near $q = 0$. The SEA setup was realized by replacing the cylinder-type spring-damper element with a spring element.

- Two environmental stiffnesses are considered; $K_e = 100$, and $K_e = 10000$;
- K_j is varied from 100 to 500 with a step size of 100;
- σ is varied from 3 to 8 with a step size of 1.

Note that the condition (39) guarantees stable interaction with any passive environments. Namely, the closed-loop including the passive environment should remain stable for any K_e. For each K_e, we investigate whether the resulting response is stable or not using every combination of K_j and σ.

For the given problem setup, condition (39) becomes

$$\sigma^2 - \sigma - (5 + 0.1K_j) > 0. \tag{48}$$

In Fig. 8, the marks 'o' and 'x' are used to denote stable and unstable responses, respectively, for each combination of K_j and σ. The right side of the orange curve satisfies (48), while the left side does not.

As shown in Fig. 8a, the condition (48) is conservative because it is a sufficient condition. Violation of the condition does not necessarily imply an unstable environmental interaction. In contrast, when interacting with a stiffer environment ($K_e = 10000$), the condition is quite tight, as shown in Fig. 8b. An important message here is that, in any case, the condition gives a guarantee for stable interaction with any passive environments.

With this message in mind, it is interesting to more closely investigate the borderline cases (i.e., when condition (48) is barely met). To investigate this, we let $K_j = 200$ and $K_e = 10000$, which requires $\sigma > 5.5$ to satisfy (48). As shown in Fig. 9, $\sigma = 5$ results in a slowly diverging response, and $\sigma = 6$ results in a slowly converging response. From the passivity point of view, $\sigma = 5$ generates the energy gradually, whereas $\sigma = 6$ can dissipate the energy but only very slowly. The dissipation becomes more visible when we increase the gain

TABLE II
SYSTEM PARAMETERS

Description	Symbol	Value
Motor side inertia	B	$1.62\ \mathrm{kg \cdot m^2}$
Link side inertia	M	$1\ \mathrm{kg \cdot m^2}$
Joint stiffness	K_j	$400\ \mathrm{Nm/rad}$
Joint damping	D_j	10 (0 for SEA) $\mathrm{Nm \cdot s/rad}$
Coulomb friction	$\cdot$	$12\ \mathrm{Nm}$
Viscous friction	$\cdot$	$10\ \mathrm{Nm \cdot s/rad}$
End stop stiffness	$\cdot$	$10000\ \mathrm{Nm/rad}$
Motor saturation	$\cdot$	$\pm 100\ \mathrm{Nm}$

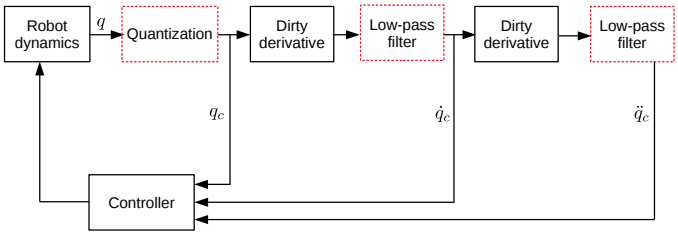

Fig. 11. Schematic diagram of simulation implementation. The velocity ($\dot{q}_c$) and acceleration ($\ddot{q}_c$) used for the controller are obtained using numerical differentiation. When quantization is considered, low-pass filters should be introduced to deal with noisy differentiation.

to $\sigma = 7$. We report that all $\sigma = 5, 6, 7$ show stable responses when there are no environmental interactions (i.e., $\tau_{ext} = 0$ with $K_e = 0$). Again, the condition guarantees stability even when the loop is closed by the passive environment around the I/O pair $(\tau_{ext}, \dot{q})$; see Fig. 4.

B. Validation with main scenario

The simulation study presented in the previous section supports the theoretical analysis with an ideal setup. In contrast, this section focuses on the scenario presented in Section I-C with a practical setup. Namely, joint friction, motor input saturation, quantization noise, and a collision that induces a large acceleration/jerk are considered.

This section presents simulations and experiments using the hardware shown in Fig. 10 with the system parameters in Table II.[6] The controller is implemented with 3 kHz frequency for both simulation and experiment. In the simulations, the end-stopper is realized by a pure spring with $10000\ \mathrm{Nm/rad}$ stiffness. Considering the scenario of interest, the following sequence of control is applied.

(i) At the beginning, the initial position is $q \simeq 0$ rad, and the desired position is set stepwise as $q_d = -0.2$ rad.
(ii) While the position stays at $q = -0.2$ rad, a human operator applies an external torque to see if impedance behavior is realized.
(iii) The desired position is suddenly changed to $q_d = 0.2$ rad (step command), which the link cannot achieve due to the end stopper; i.e., a collision occurs.

In the simulation, the human interaction is realized by applying a $10\ \mathrm{Nm}$ external torque. Note that at step (iii), the link may bounce off of the end-stopper after colliding with it, but the magnitude of each subsequent bounce should decrease, as addressed in Section I-C. Otherwise, from the passivity point of view, energy is generated during the collision, which indicates an unstable environmental interaction.[7] We emphasize that the control gains used in this section always satisfy the passivity/stability conditions.

1) Simulations: In the simulation, acceleration signal $\ddot{q}$ is obtained by taking the double derivative of q. Due to quantization (1 arcsec resolution), the quality of the acceleration signal may be significantly reduced, and an issue with the robustness may arise. To cope with the quantization noise, discretized 1st order low-pass filters are applied. In this section, subscript 'c' is used when the real signals and the signals used for the controllers should be distinguished, as shown in Fig. 11.

Fig. 12a shows the simulation result for the SEA TC-DF with $\sigma = 21.5443$ (i.e., $L_d = 464.2/K_j$, $L_p = L_i = 10000/K_j$), $K_p = 100\ \mathrm{Nm/rad}$ and $K_d = 20\ \mathrm{Nm \cdot s/rad}$. The resulting link-side behavior is reasonable at the beginning, but the collision (after $t = 6$ s) causes unacceptable behavior. The main reason for this result is that the large gain of $L_d K_d = 9283.178$ is multiplied by $\ddot{q}_c$ signal, which has a large deviation from the real $\ddot{q}$ signal (see the fifth row of Fig. 12a). To overcome this, either L_d or K_d (or even both) have to be reduced. To maintain torque tracking performance, K_d is reduced to $K_d = 5$ without changing L_d. With the reduced gain, the resulting behavior is stable after collision, as shown in Fig. 12b. In contrast, when the SvEA TC-DF is implemented with $\sigma = 21.5443$ (i.e., $L_d = 0$, $L_p = 464.2/D_j$, $L_i = 10000/D_j$), the system behaves reasonably without reducing K_d, as shown in Fig. 13.

From the simulation studies, we can observe that interaction stability of the SEA case is jeopardized when a highly dynamic motion is involved. Even when the gains are chosen according to the theoretical analysis, there is a trade-off between achievable control gains and robustness against collision. In contrast, because the quantization does not significantly degrade the quality of the velocity signal $\dot{q}_c$, the use of an SvEA can alleviate the trade-off issue arising for an SEA TC-DF. As a result, the control gains chosen according to the analysis can be used.

2) Experiments: SEA TC-DF was implemented in real hardware, with the gains summarized in Table III. $K_p = 100\ \mathrm{Nm/rad}$ and $K_d = 5\ \mathrm{Nm \cdot s/rad}$ were selected to reduce the amplification of the acceleration feedback, as discussed in the simulation studies. However, in addition to this, the torque control gains had to be reduced because $\sigma = 21.5443$ (which was used in simulation) resulted in failure in experiments; in this section, as summarized in Table III, we used $\sigma = 11.4471$ as the high gain set and $\sigma = 10$ as the low gain set.

When the high gain set was used, as shown in Fig. 14a, the impedance behavior seemed to be realized during the free motion and during gentle interaction with a human operator. However, link-side behavior became unreasonable after the

[6]The value of B is reflected through the 1:100 gear transmission.

[7]To motivate the importance of this argument, assume that the proposed control scheme is employed for the walking of a biped robot. The motion of a foot (or a leg) should be damped quickly after each touchdown. Otherwise, failure of walking may occur.

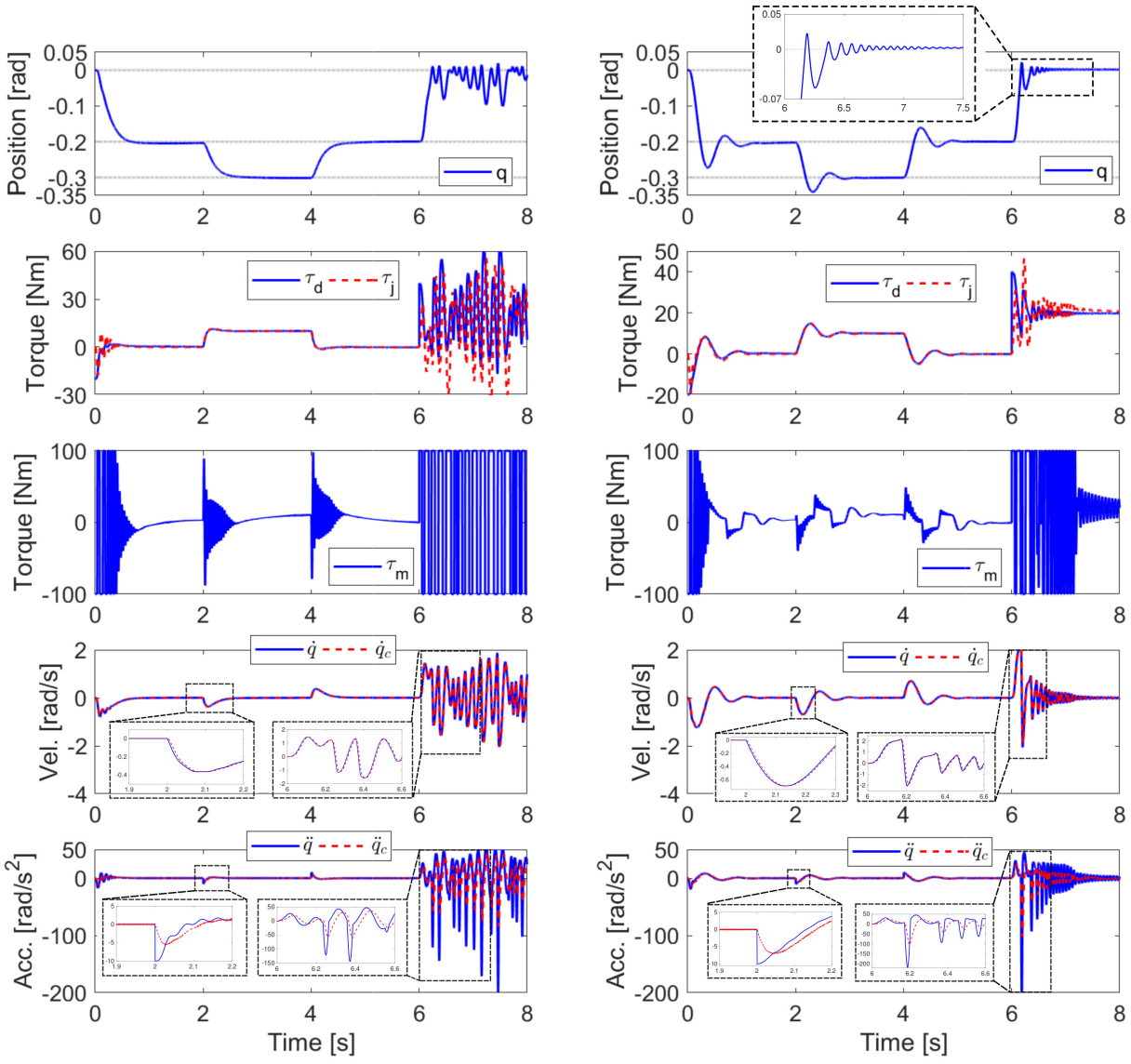

(a) $K_p = 100$ and $K_d = 20$ are used.

(b) $K_p = 100$ and $K_d = 5$ are used.

Fig. 12. Simulation results for SEA TC-DF with quantization, which results in a large discrepancy in the acceleration calculation. Because the SEA TC-DF utilizes amplified acceleration feedback, this discrepancy may deteriorate the resulting link-side behavior. (a) $K_d = 20$ is used as previously, but the resulting behavior is not stable. (b) To reduce the acceleration amplification, K_d is reduced to 5, and the resulting behavior is stable.

collision with the end-stop. To realize stable environmental interaction, the control gain was further reduced to the low gain set. Using these control gains, stable behavior during the collision could be achieved (the first row of Fig. 14b).

In contrast, when the SvEA TC-DF was implemented, we could achieve stable environmental interaction without reducing the control gains (Fig. 15). Namely, $K_p = 100$ Nm/rad and $K_d = 20$ Nm $\cdot$ s/rad were used without reducing the torque control gains, as shown in Table III. As a result, rather precise torque tracking could be achieved with stable behavior after collision.

The experimental results confirm our observations from the simulation studies. As a result, SvEA enables to realize link-side impedance controller robustly with enhanced inner-loop torque controller for stable environmental interactions even under highly dynamic motions.

VI. Summary, Conclusion, and Future Work

The main goal of this paper is to realize a link-side passive impedance controller via an inner-loop torque controller. Namely, this paper is interested in designing an inner-loop torque controller while satisfying the passivity/stability requirements of the impedance controller. This paper begins with a control structure, from which we can perform passivity/stability analysis. As a result, certain gain conditions are

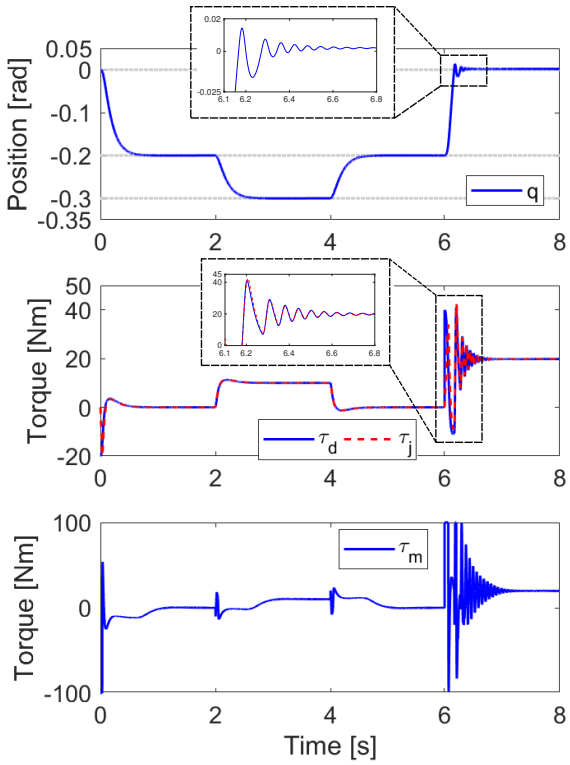

Fig. 13. Simulation results for SvEA TC-DF with quantization. Since D-control is not needed for the SvEA TC-DF, the resulting link-side behavior is stable without reducing any gains.

TABLE III
CONTROL GAINS USED IN EXPERIMENTS

			high gain	low gain
SEA	Torque control gains	σ	11.4471	10
		L_d	$131.0361/K_j$	$100/K_j$
		L_p	$1500/K_j$	$1000/K_j$
		L_i	$1500/K_j$	$1000/K_j$
	Impedance control gains	K_p	100	
		K_d	5	
SvEA	Torque control gains	σ	21.5443	·
		L_p	$464.1589/D_j$	·
		L_i	$10000/D_j$	·
	Impedance control gains	K_p	100	·
		K_d	20	·

derived, (25)-(27) for SEA and (39) for SvEA. When the SEA is considered as a joint drive, the analysis requires a D-control term, which amplifies the acceleration signals with the control gains (which are typically selected to be large). To alleviate this problem, the SvEA is introduced to reduce the acceleration amplification in the inner-loop torque control design.

Our simulation study shows that the presented theoretical analysis is correct. However, because the quality of the acceleration signal is limited by quantization, its amplification with the control gains may jeopardize the analysis in real implementations. In simulation and experimental studies, we observed that SEAs exhibit a trade-off between the achievable gains and robustness against collision. Even if the gains are set according to the theoretical analysis, stable interaction is not guaranteed when a highly dynamic motion (such as a collision) is involved. In contrast, the theoretical analysis is valid for SvEAs in real implementations because the acceleration signals are not amplified by any of the control gains. To conclude, the presented study shows that the joint viscous effect, which is often neglected, should be explicitly included in hardware design, modeling, and analysis.

A number of future works remain to be persued. For example, (i) despite the fact that some amount of viscous effect can be beneficial in principle, "some amount" is still vague. The criteria on the damping values depending on the application are worth studying. (ii) Intuitively (and also empirically), it is often believed that passivity provides robustness against input saturation. The passivity-based approach tries to dissipate energy, and saturated input implies that the controller is trying to dissipate more power than the actuator can dissipate. Some studies theoretically support this intuition [48], [49]. However, there are no further generalized findings that can be applied to the proposed control scheme. Because the main topic of this paper is passivity and stability, analysis of the input saturation remains a future work. (iii) Since our system is equipped with a large gear reduction, the friction effect may degrade the control performance. In the future, the friction observer (e.g., [7]) will be considered. (iv) As stated earlier, a variable damping actuator can be employed to span wide system characteristics. This topic may raise many questions regarding design and control problems. (v) The analysis of this paper is limited to decoupled joint stiffness/viscosity. Relaxation of this condition is remained as a future work. (vi) This paper presented a joint space impedance controller, while task space control might also be interesting for some applications.

REFERENCES

[1] M. Zinn, O. Khatib, B. Roth, and J. K. Salisbury, "Playing it safe [human-friendly robots]," Robotics & Automation Magazine, IEEE, vol. 11, no. 2, pp. 12–21, 2004.

[2] S. Haddadin, F. Huber, and A. Albu-Schäffer, "Optimal control for exploiting the natural dynamics of variable stiffness robots," in IEEE International Conference on Robotics and Automation (ICRA), 2012, pp. 3347–3354.

[3] K. Kong, J. Bae, and M. Tomizuka, "A compact rotary series elastic actuator for human assistive systems," Mechatronics, IEEE/ASME Transactions on, vol. 17, no. 2, pp. 288–297, 2012.

[4] J. Arata, K. Ohmoto, R. Gassert, O. Lambercy, H. Fujimoto, and I. Wada, "A new hand exoskeleton device for rehabilitation using a three-layered sliding spring mechanism," in IEEE International Conference on Robotics and Automation (ICRA), 2013, pp. 3902–3907.

[5] Y. Park, N. Paine, and S. Oh, "Development of force observer in series elastic actuator for dynamic control," IEEE Transactions on Industrial Electronics, vol. 65, no. 3, pp. 2398–2407, 2018.

[6] J. Lee, C. Lee, N. Tsagarakis, and S. Oh, "Residual-based external torque estimation in series elastic actuators over a wide stiffness range: Frequency domain approach," IEEE Robotics and Automation Letters, vol. 3, no. 3, pp. 1442–1449, 2018.

[7] M. J. Kim, F. Beck, C. Ott, and A. Albu-Schäffer, "Model-free friction observers for flexible joint robots with torque measurements," IEEE Transactions on Robotics, 2019.

[8] A. Albu-Schaffer and G. Hirzinger, "State feedback controller for flexible joint robots: A globally stable approach implemented on dlr's light-weight robots," in IEEE/RSJ International Conference on Intelligent Robots and Systems (IROS), vol. 2, 2000, pp. 1087–1093.

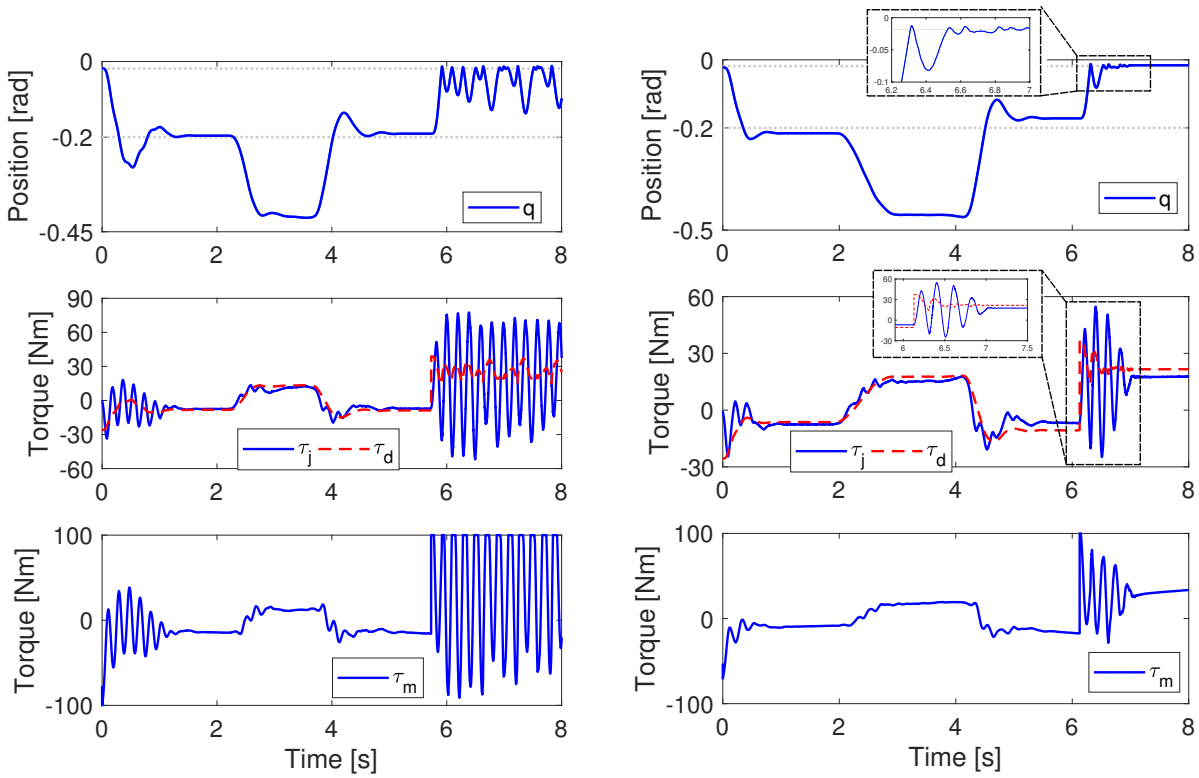

(a) SEA TC-DF with high gain set in Table III.

(b) SEA TC-DF with low gain set in Table III.

Fig. 14. Experimental result for SEA TC-DF. (a) High gain set is used. (b) Low gain set is used.

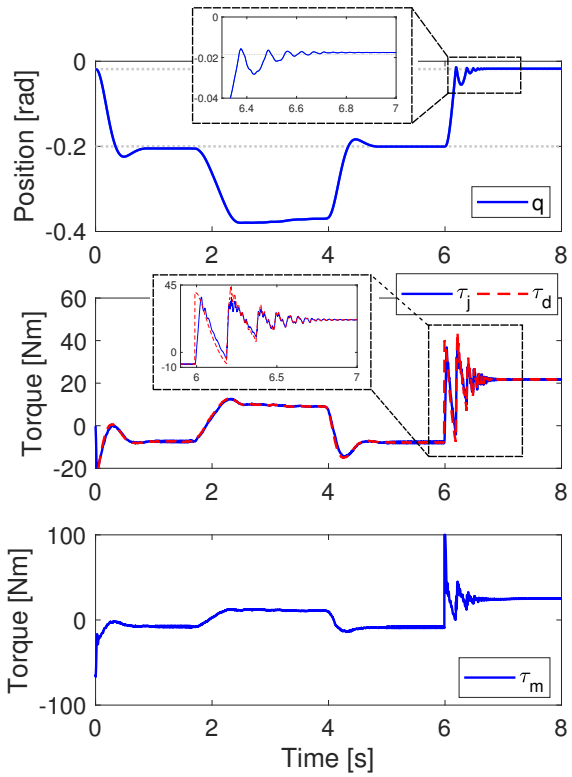

Fig. 15. Experimental results for SvEA TC-DF with the gain set in Table III.

[9] A. Albu-Schäffer, C. Ott, and G. Hirzinger, "A unified passivity-based control framework for position, torque and impedance control of flexible joint robots," The International Journal of Robotics Research, vol. 26, no. 1, pp. 23–39, 2007.

[10] C. Ott, A. Albu-Schaffer, A. Kugi, and G. Hirzinger, "On the passivity-based impedance control of flexible joint robots," Robotics, IEEE Transactions on, vol. 24, no. 2, pp. 416–429, 2008.

[11] M. J. Kim and W. K. Chung, "Disturbance-observer-based pd control of flexible joint robots for asymptotic convergence," Robotics, IEEE Transactions on, vol. 31, no. 6, pp. 1508–1516, 2015.

[12] A. Albu-Schaffer, C. Ott, and G. Hirzinger, "A passivity based cartesian impedance controller for flexible joint robots-part ii: Full state feedback, impedance design and experiments," in IEEE International Conference on Robotics and Automation (ICRA), vol. 3, 2004, pp. 2666–2672.

[13] A. De Luca and P. Lucibello, "A general algorithm for dynamic feedback linearization of robots with elastic joints," in IEEE International Conference on Robotics and Automation (ICRA), vol. 1, 1998, pp. 504–510.

[14] A. De Luca, "Feedforward/feedback laws for the control of flexible robots," in IEEE International Conference on Robotics and Automation (ICRA), vol. 1, 2000, pp. 233–240.

[15] K. Haninger and M. Tomizuka, "Robust passivity and passivity relaxation for impedance control of flexible-joint robots with inner-loop torque control," IEEE/ASME Transactions on Mechatronics, vol. 23, no. 6, pp. 2671–2680, 2018.

[16] H. Vallery, R. Ekkelenkamp, H. Van Der Kooij, and M. Buss, "Passive and accurate torque control of series elastic actuators," in IEEE/RSJ International Conference on Intelligent Robots and Systems (IROS), 2007, pp. 3534–3538.

[17] T. Boaventura, M. Focchi, M. Frigerio, J. Buchli, C. Semini, G. A. Medrano-Cerda, and D. G. Caldwell, "On the role of load motion compensation in high-performance force control," in IEEE/RSJ International Conference on Intelligent Robots and Systems (IROS), 2012, pp. 4066–4071.

[18] N. Paine, J. S. Mehling, J. Holley, N. A. Radford, G. Johnson, C.-L. Fok, and L. Sentis, "Actuator control for the nasa-jsc valkyrie humanoid robot: A decoupled dynamics approach for torque control of series

elastic robots," Journal of Field Robotics, vol. 32, no. 3, pp. 378–396, 2015.
[19] W. Lee, M. J. Kim, and W. K. Chung, "Model-free joint torque control strategy for hydraulic robots," in IEEE International Conference on Robotics and Automation (ICRA), 2016, pp. 2408–2415.
[20] K. Kong, J. Bae, and M. Tomizuka, "Control of rotary series elastic actuator for ideal force-mode actuation in human–robot interaction applications," IEEE/ASME transactions on mechatronics, vol. 14, no. 1, pp. 105–118, 2009.
[21] S. Yoo and W. K. Chung, "Sea force/torque servo control with model-based robust motion control and link-side motion feedback," in IEEE International Conference on Robotics and Automation (ICRA), 2015, pp. 1042–1048.
[22] S. Oh and K. Kong, "High-precision robust force control of a series elastic actuator," IEEE/ASME Transactions on Mechatronics, vol. 22, no. 1, pp. 71–80, 2017.
[23] C. Lee and S. Oh, "Robust assistive force control of leg rehabilitation robot," in IEEE International Conference on Advanced Intelligent Mechatronics (AIM), 2017, pp. 634–638.
[24] M. Focchi, G. A. Medrano-Cerda, T. Boaventura, M. Frigerio, C. Semini, J. Buchli, and D. G. Caldwell, "Robot impedance control and passivity analysis with inner torque and velocity feedback loops," Control Theory and Technology, vol. 14, no. 2, pp. 97–112, 2016.
[25] Y. Zhao, N. Paine, S. J. Jorgensen, and L. Sentis, "Impedance control and performance measure of series elastic actuators," IEEE Transactions on Industrial Electronics, vol. 65, no. 3, pp. 2817–2827, 2018.
[26] G. Wyeth, "Demonstrating the safety and performance of a velocity sourced series elastic actuator," in IEEE International Conference on Robotics and Automation (ICRA), 2008, pp. 3642–3647.
[27] D. P. Losey, A. Erwin, C. G. McDonald, F. Sergi, and M. K. O'Malley, "A time-domain approach to control of series elastic actuators: Adaptive torque and passivity-based impedance control," IEEE/ASME Transactions on Mechatronics, vol. 21, no. 4, pp. 2085–2096, 2016.
[28] D. Kim, Y. Zhao, G. Thomas, B. R. Fernandez, and L. Sentis, "Stabilizing series-elastic point-foot bipeds using whole-body operational space control," IEEE Transactions on Robotics, vol. 32, no. 6, pp. 1362–1379, 2016.
[29] N. L. Tagliamonte, D. Accoto, and E. Guglielmelli, "Rendering viscoelasticity with series elastic actuators using cascade control," in IEEE International Conference on Robotics and Automation (ICRA), 2014, pp. 2424–2429.
[30] J. S. Mehling, "Impedance control approaches for series elastic actuators," Ph.D. dissertation, Rice University, 2015.
[31] M. Mosadeghzad, G. A. Medrano-Cerda, J. A. Saglia, N. G. Tsagarakis, and D. G. Caldwell, "Comparison of various active impedance control approaches, modeling, implementation, passivity, stability and trade-offs," in IEEE/ASME International Conference on Advanced Intelligent Mechatronics (AIM), 2012, pp. 342–348.
[32] M. Laffranchi, L. Chen, N. G. Tsagarakis, and D. G. Caldwell, "The role of physical damping in compliant actuation systems," in IEEE/RSJ International Conference on Intelligent Robots and Systems (IROS), 2012, pp. 3079–3085.
[33] D. Kim, J. Ahn, O. Campbell, N. Paine, and L. Sentis, "Investigations of a robotic test bed with viscoelastic liquid cooled actuators," IEEE/ASME Transactions on Mechatronics, vol. 23, no. 6, pp. 2704–2714, 2018.
[34] C.-M. Chew, G.-S. Hong, and W. Zhou, "Series damper actuator: a novel force/torque control actuator," in 4th IEEE/RAS International Conference on Humanoid Robots, vol. 2, 2004, pp. 533–546.
[35] M. Laffranchi, N. G. Tsagarakis, and D. G. Caldwell, "A variable physical damping actuator (vpda) for compliant robotic joints," in IEEE International Conference on Robotics and Automation (ICRA), 2010, pp. 1668–1674.
[36] M. Laffranchi, N. Tsagarakis, and D. G. Caldwell, "A compact compliant actuator (compact™) with variable physical damping," in IEEE International Conference on Robotics and Automation (ICRA), 2011, pp. 4644–4650.
[37] M. J. Kim, A. Werner, F. C. Loeffl, and C. Ott, "Enhancing joint torque control of series elastic actuators with physical damping," in IEEE International Conference on Robotics and Automation (ICRA), 2017, pp. 1227–1234.
[38] C. C. De Wit, G. Bastin, and B. Siciliano, Theory of robot control. Springer-Verlag New York, Inc., 1996.
[39] R. Sepulchre, M. Jankovic, and P. V. Kokotovic, Constructive nonlinear control. Springer Science & Business Media, 2012.
[40] A. J. van der Schaft and A. Van Der Schaft, L2-gain and passivity techniques in nonlinear control. Springer, 2000, vol. 2.
[41] H. K. Khalil and J. Grizzle, Nonlinear systems. Prentice hall Upper Saddle River, 2002, vol. 3.
[42] G. Garofalo, N. Mansfeld, J. Jankowski, and C. Ott, "Sliding mode momentum observers for estimation of external torques and joint acceleration," in IEEE International Conference on Robotics and Automation (ICRA), 2019, pp. 6117–6123.
[43] T. Boaventura, J. Buchli, C. Semini, and D. G. Caldwell, "Model-based hydraulic impedance control for dynamic robots," IEEE Transactions on Robotics, vol. 31, no. 6, pp. 1324–1336, 2015.
[44] G. Pratt and M. Williamson, "Series elastic actuators," in IEEE/RSJ International Conference on Intelligent Robots and Systems (IROS), vol. 1, Aug 1995, pp. 399–406 vol.1.
[45] A. Calanca and P. Fiorini, "A rationale for acceleration feedback in force control of series elastic actuators," IEEE Transactions on Robotics, 2018.
[46] C. Ott, A. Albu-Schaffer, A. Kugi, and G. Hirzinger, "Decoupling based cartesian impedance control of flexible joint robots," in IEEE International Conference on Robotics and Automation (ICRA), vol. 3, 2003, pp. 3101–3107.
[47] C. Ott, Cartesian impedance control of redundant and flexible-joint robots. Springer, 2008.
[48] A. Loria, R. Kelly, R. Ortega, and V. Santibanez, "On global output feedback regulation of euler-lagrange systems with bounded inputs," IEEE Transactions on Automatic Control, vol. 42, no. 8, pp. 1138–1143, 1997.
[49] A. Zavala-Rio and V. Santibanez, "Simple extensions of the pd-with-gravity-compensation control law for robot manipulators with bounded inputs," IEEE Transactions on Control Systems Technology, vol. 14, no. 5, pp. 958–965, 2006.

Min Jun Kim received the B.S. degree in mechanical engineering from Korea University, in 2010, and received the Ph.D. degree in mechanical engineering from Pohang University of Science & Technology (POSTECH), in 2016. From June 2016 to July 2020, he was working as a research scientist in the Institute of Robotics and Mechatronics, German Aerospace Center (DLR). He is currently an assistant professor of Electrical Engineering at Korea Advanced Institute of Science and Technology (KAIST). His research interests include flexible joint robots, physical robot interaction, aerial robots, nonlinear robust control.

Alexander Werner received the Dipl.-Ing. degree in mechatronics engineering from the University of Erlangen-Nuremberg. When he worked for the German-Aerospace center (DLR), he focussed on optimal control for efficient locomotion and effective use of elastic actuators. Currently he is with the University of Waterloo, as a research associate and works on the locomotion control and control of elastic structures.

FLorian Loeffl received his Dipl.Ing. Degree in Mechanical Engineering from Technical University of Munich, Germany, in 2008. He joined the German Aerospace Center (DLR) in 2014 as leader of the development team of the elastic bipedal robot C-Runner. Since 2017 he is head of the systems design group at DLRs Institute of Robotics and Mechatronics. His current research interests include modular systems engineering and elastically actuated legged robots.

Christian Ott received the Dipl.-Ing. degree in mechatronics from Johannes Kepler University, Linz, Austria, in 2001 and the Dr.-Ing. degree in control engineering from Saarland University, Saarbruecken, Germany, in 2005. From 2001 to 2007, he was with the Institute of Robotics and Mechatronics, German Aerospace Center (DLR), Wessling, Germany. From May 2007 to June 2009, he was working as a Project Assistant Professor with the Department of Mechano-Informatics, University of Tokyo, Tokyo, Japan. From 2011 to 2016, he has been working with DLR as a Team Leader with the Helmholtz Young Investigators Group for Dynamic Control of Legged Humanoid Robots. Since 2014, he has been the Head with the Department of Analysis and Control of Advanced Robotic Systems, DLR. His current research interests include nonlinear robot control, flexible joint robots, impedance control, and control of humanoid robots.